

Self-Supervised Time-to-Event Modeling with Structured Medical Records

Ethan Steinberg, Yizhe Xu, Jason Fries, Nigam Shah

June 26, 2023

Abstract

Time-to-event (TTE) models are used in medicine and other fields for estimating the probability distribution of the time until a specific event occurs. TTE models provide many advantages over classification using fixed time horizons, including naturally handling censored observations, but require more parameters and are challenging to train in settings with limited labeled data. Existing approaches, e.g. proportional hazards or accelerated failure time, employ distributional assumptions to reduce parameters but are vulnerable to model misspecification. In this work, we address these challenges with MOTOR (Many Outcome Time Oriented Representations), a self-supervised model that leverages temporal structure found in collections of timestamped events in electronic health records (EHR) and health insurance claims. MOTOR uses a TTE pretraining objective that predicts the probability distribution of times when events occur, making it well-suited to transfer learning for medical prediction tasks. Having pretrained on EHR and claims data of up to 55M patient records (9B clinical events), we evaluate performance after finetuning for 19 tasks across two datasets. Task-specific models built using MOTOR improve time-dependent C statistics by 4.6% over state-of-the-art while greatly improving sample efficiency, achieving comparable performance to existing methods using only 5% of available task data.

1 Introduction

Many applications in medicine require predicting not only the overall likelihood of an event, but also when that event will occur. *Time-to-event (TTE) models* (also called *survival models*) are commonly used to estimate the probability distribution of TTE data given a set of features. TTE models have two primary advantages over standard classification approaches using fixed time horizons. First, they can estimate temporal quantities of interest such as the hazard rate or the median time until an event occurs. Second, TTE models account for various types of censoring induced by different data collection mechanisms, which is critical for obtaining accurate estimates and fair models [7]. TTE models are commonly used, *inter alia*, in medicine [1, 14, 34, 38], for churn prediction [47], real time advertisement bidding [68], recommendation systems [27], and other business analytics.

Despite the benefits of TTE models, they come with the downside of requiring large training sets in order to estimate the entire TTE probability distribution. High censoring rates, common in medical events with long time horizons, further limit the available training data and exacerbate the risk of overfitting. A variety of methods have been proposed to mitigate this issue, generally by making assumptions about the TTE distribution such as proportional hazards [10] or parametric

distributions [39, 4]. These assumptions significantly reduce the number of learnable parameters, but may also degrade predictive performance when they do not hold [57].

Recent work in deep learning has approached the challenge of limited training data by relying on transfer learning via increasingly powerful *foundation models* [5]. Foundation models leverage advances in self-supervised learning to train models using large collections of unlabeled data. The resulting pretrained models learn broadly useful features that can then be rapidly adapted to new tasks via finetuning, substantially lowering the amount of labeled data and time required to train task-specific models. Self-supervised learning requires specifying a pretraining task that captures useful patterns from the unlabeled data, typically by predicting some intrinsic property of the data itself. For example, autoregressive pretraining in Natural Language Processing (NLP) predicts the next word in a sequence conditioned on prior words [49].

Structured medical records, e.g. electronic health records (EHR) and insurance claims data, consist of sequences of timestamped events, where each event consists of a clinical code drawn from a finite symbol vocabulary defined by medical terminologies. This “language”, comprised of a sequence of clinical codes rather than words, is conducive to autoregressive pretraining and its use has resulted in strong predictive performance and improved sample efficiency in building fine-tuned models for several medical tasks [61]. However, large-scale pretraining is under-explored for TTE modeling, and the benefits of scaling remain unclear. It is also uncertain how well transfer learning using standard autoregressive objectives works for TTE modeling since it disregards much of the temporal structure present in structured medical records.

In this work, we introduce MOTOR (Many Outcome Time Oriented Representations), whose main contributions are:

1. A self-supervised pretraining objective that uses thousands of TTE tasks (8,192 in our experiments) during pretraining to learn broadly useful features for TTE modeling.
2. An efficient Transformer-based piecewise exponential model architecture that leverages shared time-dependent weights and sparse operations to scale to thousands of TTE pretraining tasks.
3. Experiments on EHR and claims data demonstrating that TTE pretraining improves accuracy and data efficiency, with on average 4.6% accuracy improvement over state-of-the-art methods for 19 evaluation tasks when using the full dataset and comparable performance to existing methods using only 5% of available task data.
4. MOTOR model weights pretrained on EHR data, released for non-commercial research use to help address reproducibility challenges in current medical foundation models [67].

2 Related Work

2.1 Time-to-event Models

Accelerated failure time (AFT) models are a fully parametric approach for modeling TTE outcomes where the TTE distribution is parameterized with a specified probability distribution. AFT models assume that the parameters of that specified probability distribution are a learnable function of the features. Common probability distributions include exponential, gamma, log-normal, log-logistic, and Weibull. Piecewise distributions enable the use of different distribution parameters across different regions of time and thus provide additional flexibility, with the piecewise exponential

distribution [16] being a popular choice. More recently, AFT models have been combined with deep learning by using a neural network to map between input features and distribution parameters [15, 39, 54, 31, 4, 33].

Cox proportional hazards (PH) models [10] reduce the complexity of the model space by assuming a constant hazard ratio between instances over time. In situations where the PH assumption does not hold, Cox PH models may perform poorly. Cox models can also be combined with deep learning by using a neural network to map between the input features and the learned constant hazard ratio [28].

Random survival forests (RSFs) [26] are a nonparametric approach that extends random forests [6] to TTE tasks. RSFs estimate cumulative hazard functions using the Nelson-Aalen estimator. The best splitting variable at each node is selected to maximize the survival differences between the two daughter nodes. Similar to random forests, RSFs automatically identify nonlinear relationships among variables via the recursive partitioning scheme and apply bagging, random subsampling, and random variable selection techniques to improve model performance. Athey et al. [2] further introduces “honest” trees for building RSFs to mitigate overfitting in which separate data sets are used for tree construction and prediction. One major limitation of RSFs is that they are computationally inefficient when applied to large-scale data [52].

Some work has explored using multi-task learning to better fit TTE models in cases with limited data. Li et al. [36] proposed treating the pieces in piecewise TTE models as instances of related tasks and regularizing models to share weights across pieces. Gao and Cui [17] explored choosing “compatible” clinical tasks (i.e., clinical tasks with similar risk structure) to better learn neural network featurized Cox models. Wang and Sun [65] evaluated learning mortality and length of stay models simultaneously while training cancer models. MOTOR differs from these approaches in several ways. First, we focus on a self-supervised pretraining objective that captures temporal structure from general clinical events. Second, we dramatically increase the scale of patients (up to 55M) and tasks (8,192 tasks) and outline methods required to efficiently train at this scale. Finally, we explore the benefits of this pretraining on various downstream tasks.

2.2 Deep Learning for Structured Medical Record Data

There is considerable prior work using deep learning with structured medical records to train models for medical classification tasks. Early approaches, best exemplified by DeepPatient [41] and the feedforward model in Rajkomar et al. [51], were analogous to bag-of-words featurization in NLP and required transforming patient medical record data into sparse, count-based feature matrices. While parameter efficient, these approaches require manual (and non-obvious) feature engineering choices to capture temporal information about events. Recent architectures directly incorporate the temporal structure of medical record data by using recurrent neural networks (RNNs) [8, 9] or attention-based models such as Transformers [37]. These time-oriented neural network models use sequential structured inputs to model interactions between medical events over time.

While prior deep learning methods trained models end-to-end using small, task-specific cohorts, recent work uses self-supervised learning to pretrain models using millions of patient records [53]. The resulting foundation models demonstrate strong transfer learning properties including improved accuracy, sample efficiency, and temporal robustness [20] via finetuning and other adaptation techniques. Various self-supervised objectives have been proposed for learning meaningful patterns in structured medical record data. DeepPatient used a denoising autoencoder objective to learn effective feedforward models. CLMBR [61] pretrained an RNN using an autoregressive, “next day”

code prediction task (analogous to language modeling in NLP). Other work has used masked language modeling objectives to predict “corrupted” tokens in EHR input streams [37, 53, 46, 70].

The majority of these architectures are formulated for classification tasks with fixed time horizons, e.g., 3-12 month mortality [3]. However, there are several efforts that combine deep learning with TTE modeling on EHR data. Avati et al. [4] used RNNs and feedforward neural networks to power AFT models for estimating time until death. Rasmy et al. [52] used RNNs to train Cox models for hospital mortality and ventilation need. Wen et al. [66] used feedforward networks to parameterize Cox and DeepHIT [56] models for predicting time until discharge. MOTOR differs from these prior works in two ways: 1) We use a Transformer-based piecewise exponential model to handle complex and nonlinear relationships in data, and 2) we leverage TTE pretraining at a massive scale to estimate model parameters more effectively.

3 Methods

3.1 Problem Setup

We consider a set of N patients and their medical records X , where X_i denotes patient i ’s information and consists of a sequence of timestamped events, where each event is defined by a code that is a symbol drawn from a finite set defined by standard medical ontologies [58]. For example, many research datasets use ICD-10 codes [44] to indicate diseases, CPT codes [13] to indicate procedures, RxNorm codes [42] to indicate drugs, and so forth. Let X_{ij} denote the j -th event in the sequence, where each event consists of a code for that event and the corresponding timestamp for when that event occurs. In this work, we only consider coded data and discard clinical notes and other unstructured data.

We are interested in learning models to predict TTE tasks for patients in our dataset. Let T_i and C_i denote the event time and censoring time for patient i , respectively. $U_i = \min(T_i, C_i)$ is the observed follow-up time and $\delta_i = \mathbb{1}\{T_i \leq C_i\}$ is the event indicator, which is 1 if the patient experiences the event at U_i or 0 if the patient is censored at U_i . Our estimand of interest is $\mathbb{P}(t|X_i) = \mathbb{P}(T_i = t)$ where t is an arbitrary prediction time.

3.2 MOTOR

We introduce MOTOR, a Transformer-based neural network model that is pretrained using a self-supervised, TTE objective defined using structured medical records data. Figure 1 provides an overview of our approach, where patient records are fed into a Transformer backbone and converted into latent representations that are then used during TTE pretraining. The resulting pretrained MOTOR model is then combined with a linear head to train downstream TTE models for particular tasks of interest such as predicting the time until a heart attack.

3.2.1 Transformer

Following the previous work of BEHRT [37], we use a Transformer-based neural network for processing our medical record data. X_i , the sequence of codes and timestamps for patient i , is first transformed into a combination of code and time embeddings. Code embeddings are generated with a standard embedding layer. Time embeddings are generated using a rotary position embedding [62] with time

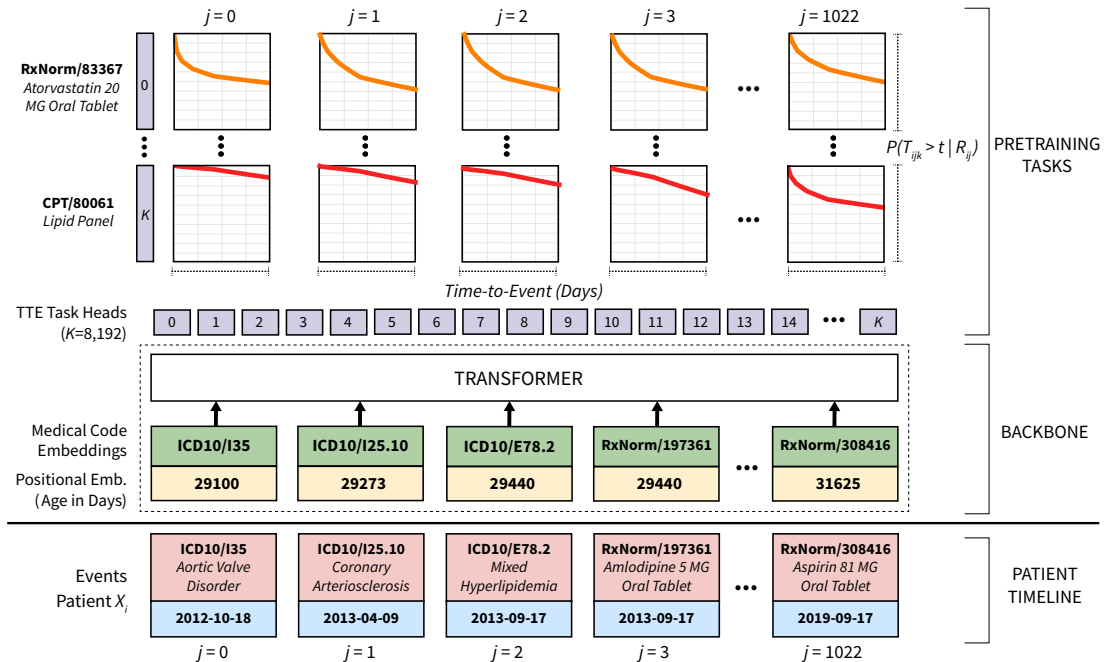


Figure 1: An overview of the MOTOR architecture and the TTE pretraining task, as applied to a single patient with 1,022 events.

(in days since birth) instead of the more standard position index. These embeddings are then fed into a Transformer to generate representations for every event in each patient’s record.

Our Transformer differs from the main prior work of BEHRT in four major aspects. First, unlike BEHRT, which uses a masked language modeling objective that incorporates bidirectional information from patient sequences, we use causally masked attention [12, 48, 50]. This attention pattern ensures information only flows forwards in the sequence and not backwards to guarantee that the model does not “cheat” by using information from the future. If fully connected attention is used instead, models quickly learn shortcuts to use future information to predict the past, which then results in failure when the models are applied to real data. Second, we use rotary position embeddings [62] for combining the time and code embeddings at every attention subunit in the network. Third, we use a local attention mechanism, where attention is limited to 512 token context windows, to enable the use of sequence lengths up to 16,384 events and avoid quadratic complexity [55]. Fourth, we do not use the explicit visit based components of BEHRT (the segment and position features) as our source medical record data contains overlapping visits that are not compatible with BEHRT’s approach. Instead, we represent visits as additional clinical events within the timeline.

The output of our model is one matrix per patient R_i , where each row R_{ij} corresponds to the patient i ’s representation for the event j that contains cumulative information up to and including event j . The width of the row R_{ij} is the size of the patient representation, which is a tunable hyperparameter.

3.2.2 Large Scale Piecewise Exponential Time-to-event Model

Given the representations computed by the Transformer, MOTOR constructs a large-scale TTE model that can generate survival predictions for thousands of tasks. We derive and implement a scalable approach based on the Piecewise Exponential Artificial Neural Networks (PEANN) [15] framework that can work with a large number of tasks.

Piecewise exponential models approximate the TTE distribution with a piecewise exponential function, with a fixed number of pieces P , with each piece covering a pre-specified region of time. For every patient i , event j , task k , and piece p , a hazard λ_{ijkp} must be estimated to compute TTE distributions for each patient. These hazard estimates λ are combined with the event indicator tensor δ (defined as δ_{ijkp} indicating whether or not subject i at the time of event j has an event for task k within the piece p) and event time tensor U (defined as U_{ijkp} being the time to either the task event or censorship within piece p for patient i , event j and task k) to construct the standard piecewise exponential likelihood loss function:

$$L(U_{ijkp}|\lambda_{ijkp}) = \{\lambda_{ijkp} \exp(-\lambda_{ijkp} U_{ijkp})\}^{\delta_{ijkp}} \{\exp(-\lambda_{ijkp} U_{ijkp})\}^{1-\delta_{ijkp}} \quad (1)$$

Computing this loss requires the evaluation of large matrix operations due to the dependence on i , j , k , and p , so we employ three optimizations to make this more tractable and reduce the number of parameters needed per task k . First, we assume that the transformation $R_{ij} \mapsto \log(\lambda_{ijkp})$ is a linear mapping of low rank, and compute it with two smaller matrix multiplications. This is done by learning a time-independent task embedding β_k of size b for each event k and learning a time-dependent linear transformation M_{ijp} from patient representation R_{ij} , in which M_{ijp} represents the state of patient i at event j within piece p . We can then compute $\log(\lambda_{ijkp}) = M_{ijp} \cdot \hat{\beta}_k$, which requires only b parameters per task. The intuition here is that tasks should largely be time-independent in the sense that diseases depend on the same set of risk factors over time. As a second optimization, we note that this pretraining task involves a high degree of censorship. A patient may have a variety of events, but the odds of a patient having a particular event are low. Thus, δ is often sparse and U contains many duplicate entries. We can implement both of those with sparse matrix operations to significantly reduce compute and memory. Finally, as we are only interested in the product of the likelihood loss function and not the individual terms, we can fuse most of the steps in a single kernel such that large matrix intermediates like λ are never fully materialized.

3.2.3 Time-to-event Pretraining Task

Given our Transformer encoder and piecewise exponential TTE model specification, we define a pretraining task of predicting the time to various events defined by codes in our medical records data. To achieve a general TTE model that captures as much signal as possible, we train on as many tasks (codes) as we can fit into GPU memory, 8,192 on our hardware. We select the 8,192 most informative codes as ranked by entropy, defined by Shannon’s formula [59].

To provide a more conservative measure of performance on novel TTE tasks, we take an additional step of explicitly removing codes for our evaluation target tasks from the set of pretraining tasks. Note that removing codes for evaluation is not strictly necessary for correctness as we are using a patient split to ensure no leakage between pretraining and evaluation.

We pretrain our model end-to-end using the likelihood in Equation (1) averaging over all 8,192 codes. We train for ten epochs using the Adam optimizer with a learning schedule defined by a

linear warmup followed by a linear learning rate decay. Hyperparameters are set through a grid search (detailed in Appendix A) on the validation set.

3.2.4 Adapting MOTOR to Target Tasks

Given the pretrained model above, we can then train models for new target tasks of interest through the process of adaptation. Specifically, we need to estimate a new vector of parameters $\hat{\beta}_k^{\text{new}}$ for the new task by minimizing the piecewise exponential loss function on the target task dataset.

We evaluate two methods of adapting MOTOR, using a linear probe (MOTOR-Probe) and full finetuning (MOTOR-Finetune). In the linear probe setup, only $\hat{\beta}_k^{\text{new}}$ are tuned for each task and no other weights are modified. This simple approach allows models to be trained rather quickly as gradients only have to be evaluated over a small fraction of the model. The linear probe approach can also in theory work for very small sample sizes as it is resistant to overfitting. Alternatively, in the full finetuning setup, all of MOTOR’s weights are updated when finetuning. This is a flexible approach that can enable higher prediction accuracy but comes at the cost of requiring increased runtime as gradients have to be computed throughout the entire model. For all of our full finetuning runs, we additionally apply the standard technique of initializing the model with a linear probe first before finetuning [32]. As an ablation, we also evaluate training MOTOR from scratch, without any adaptation (MOTOR-Scratch). In this setup, we randomly initialize MOTOR and train the whole model on the target task.

4 Experiments

We evaluate the effectiveness of MOTOR by comparing the performance of MOTOR-derived models to several state-of-the-art TTE models and under various ablations. The code for our experiments can be found within the supplement.

4.1 Datasets and Compute

We use two healthcare datasets: EHR-OMOP, a de-identified private EHR dataset from an academic medical center, and TRUVEN, the 2017 release of the de-identified Truven Health MarketScan Commercial Claims and Encounters Database [24]. EHR-OMOP contains longitudinal EHR data for adult and pediatric populations with a total of 2.7M patient records (2.4B clinical events) spanning 2014 - 2022. Each record includes demographics (age, sex, ethnicity) and medical codes for diagnoses, labs, medications, procedures, and visits. TRUVEN contains claims information (i.e., billing diagnoses, medications, procedures, and visits) for 78M patients (12.8B clinical events) spanning 2007 - 2017. Data processing and splitting details are in Appendix B, with compute information in Appendix C.

4.2 Setup of Target Tasks

We derive 19 target tasks for evaluation models. Our evaluation set consists of six code-based target tasks (predicting the time to a particular diagnosis code is assigned) and 13 text-based target tasks (predicting the time to the creation of a radiology note that refers to a particular condition). For all tasks, a prediction time is defined by choosing the end of a random visit after at least a year of medical history. For simplicity, we assume death is the only competing risk and censor each record

at death. As the number of patients in our datasets is large, we perform subsampling (primarily of low information censored examples, see Appendix D) to achieve reasonable target task sample sizes.

The six code-based tasks are Celiac Disease, Heart Attack (HA), Lupus, Nonalcoholic Fatty Liver Disease (NAFLD), Pancreatic Cancer, and Stroke. These tasks were chosen to cover a spectrum of acute and chronic health conditions. These clinical events are defined by a set of ICD-10 codes that are expanded using OMOP SNOMED based ontology mappings [58]. Per Section 3.2.3, we remove these codes (and related concepts) from pretraining to better evaluate model performance on unseen tasks. Table S4 in Appendix E lists the codes-based task definitions and the number of patients for each task. We evaluate these six tasks on both EHR-OMOP and TRUVEN.

One issue with code-based tasks is that coded data is incomplete and thus many useful tasks can only be defined using information derived from text [69]. In order to explicitly evaluate this setting, we additionally perform a separate analysis with 13 text-based tasks, using the 13 radiology note labeling functions provided by Irvin et al. [25]. The details for this setup are in Appendix H.3. We only evaluate these 13 tasks on EHR-OMOP as TRUVEN does not contain notes.

4.3 Baselines

We compare MOTOR-derived models with three state-of-the-art TTE modeling approaches that make different types of modeling assumptions: Cox PH, DeepSurv, and RSFs. Cox PH and RSFs cannot naively handle our sequential event format as they require input features to be in the form of a feature matrix. In order to run those methods on our dataset, we implement a featurization strategy to transform our timestamped event data into rows and columns that can be used for those methods. Following prior standard practice in the medical domain [43], we implement count featurization, where a column is created for each event code in the source data and each value in that column corresponds to the number of times that event code appears in the patient record.

In principle, DeepSurv can accept the same event/timestamp input format as MOTOR by using a Transformer, however we observe poor performance due to overfitting on our small task datasets. Instead, we train DeepSurv on the same feature matrices used for RSFs and Cox PH. In this way, training DeepSurv requires learning many fewer parameters and thus is less prone to overfitting. We parameterize DeepSurv with a feedforward neural network with two hidden layers, rectified linear unit (ReLU) activation functions, and batch-normalization. As in MOTOR, we use dropout and early stopping for regularization.

Appendix A contains the hyperparameter search grids as well as the software versions used.

4.4 Evaluation Metrics

We evaluate model performance using three metrics, the time-dependent C statistic [23], Harrell’s C-index [21], and the Nam-D’Agostino (ND) calibration metric [11]. The C statistics provide an estimate of ranking performance, i.e., the ability of the model to correctly rank higher-risk patients over lower-risk patients. The ND calibration provides information on whether the estimated survival curves contain correct probabilities. Details on these metrics, including how we adjust them for simultaneous events and compute statistical significance, can be found in Appendix F.

5 Results

5.1 Overall Performance

Table 1 provides the time-dependent concordance performance of the various methods trained on the full datasets for the code-based tasks. Both pretrained MOTOR variants (MOTOR-Finetune and MOTOR-Probe) generally outperform all of our baselines, providing statistically significant higher C statistics in all six code-based tasks (confidence intervals are shown in Table S5 in Appendix G). The corresponding calibration results can be found in Appendix H.1, with Harrell’s C-index in Appendix H.2.

The comparison between MOTOR-Scratch (where the model is trained from scratch only on the target task without any pretraining) versus MOTOR-Finetune is a particularly important comparison, as it directly tests the importance of pretraining. As MOTOR combines a sophisticated neural network model with pretraining, it is important to evaluate whether pretraining itself provides value. MOTOR-Scratch uses the same piecewise exponential setup, Transformer backbone, and hyperparameter grid as MOTOR-Finetune, with the only difference being that MOTOR-Scratch is trained only on the target tasks. MOTOR-Scratch performs worse, demonstrating the importance of pretraining, especially on the smaller, more feature-rich EHR-OMOP dataset.

Table 1: Time-dependent C statistic for all methods on the code-based tasks. Bolding indicates the best performing model.

Method	Dataset	Celiac	HA	Lupus	NAFLD	Cancer	Stroke
Cox PH	EHR-OMOP	0.689	0.761	0.770	0.726	0.793	0.779
DeepSurv	-	0.704	0.823	0.790	0.800	0.811	0.830
RSF	-	0.729	0.836	0.787	0.802	0.824	0.840
MOTOR-Scratch	-	0.696	0.795	0.803	0.821	0.777	0.831
MOTOR-Probe	-	0.802	0.884	0.850	0.859	0.865	0.874
MOTOR-Finetune	-	0.802	0.887	0.863	0.864	0.865	0.875
Cox PH	TRUVEN	0.538	0.783	0.749	0.799	0.628	0.693
DeepSurv	-	0.719	0.814	0.809	0.828	0.801	0.753
RSF	-	0.705	0.810	0.805	0.838	0.798	0.746
MOTOR-Scratch	-	0.737	0.821	0.826	0.850	0.821	0.775
MOTOR-Probe	-	0.755	0.828	0.833	0.856	0.825	0.789
MOTOR-Finetune	-	0.762	0.831	0.838	0.862	0.834	0.794

The performance results on the 13 text-based tasks are described in Appendix H.3, with the same pattern of MOTOR outperforming RSF.

5.2 Choice of Pretraining Objective

One of the main novel components of MOTOR is our TTE pretraining objective. In order to investigate how much this pretraining objective contributes to MOTOR’s performance, we perform a comparison with another common pretraining task: next code prediction. This autoregressive pretraining task aims to predict the next code in the timeline for each patient. A full description of

how we implemented this is contained in Appendix I, but the overall idea is similar to the standard autoregression pretraining objective commonly used in NLP language modeling.

In order to ensure a fair comparison, we use matched hyperparameter grid searches and model architectures when comparing next-code pretraining to TTE pretraining. We only perform this ablation on the smaller EHR-OMOP dataset where pretraining is the most impactful (as determined by the gap in performance between MOTOR-Finetune and MOTOR-Scratch). Finally, we only evaluate the full finetuning method on both models since next code does not support linear probing.

Table 2 compares the next code pretraining task to our TTE pretraining task on EHR-OMOP. The TTE pretraining task outperforms the next code pretraining task, as indicated by the statistically significant higher C statistics on four of the target tasks (confidence intervals in Table S6). This implies that utilizing a TTE pretraining task is beneficial for predicting TTE outcomes.

Table 2: Impact of the pretraining objective on model performance in terms of the time-dependent C statistic on the code-based tasks. We compare a “next code” baseline with our proposed TTE objective. Bolding indicates the best performing model.

Objective	Celiac	HA	Lupus	NAFLD	Cancer	Stroke
Next Code	0.774	0.862	0.842	0.860	0.860	0.857
Time-to-Event	0.802	0.887	0.863	0.864	0.865	0.875

5.3 Sample Efficiency

A key benefit of foundation models is improved sample efficiency, enabling the construction of effective task models with few labeled training examples. We evaluate MOTOR’s sample efficiency in two ways, how performance changes as we pretrain the model with fewer patients and as we adapt the model with fewer patients. To function in an academic, compute resource-constrained environment, we run all of these experiments with linear probing instead of full finetuning.

In order to evaluate the performance as a function of the amount of pretraining data, we subsample each patient database to 5%, 10%, and 25% of their original sizes and pretrain on those reduced patient sets. We then adapt each pretrained model using linear probing on all six evaluation tasks. Similarly, in order to estimate performance as a function of the size of the task-specific dataset used for adaptation, we subsample each task-specific dataset to 5%, 10%, and 25% of the original size and fit linear probes on those subsampled datasets. Figure 2 plots the time-dependent C statistic of both the pretraining and code-based target tasks for these experiments.

We find that MOTOR is robust to the amount of adaptation data available, with good performance even for a very small number of labels. On the other hand, MOTOR performance degrades quite rapidly when the pretraining dataset is reduced. This matches intuition as pretraining is the critical component that requires learning millions of weights, while adapting via a linear probe only requires estimating 512 weights for the linear head. In the same theme of investigating low resource environments, we also evaluate the compute efficiency of linear probing in Appendix H.4 and find that we can learn linear probes about ten times faster than the strongest baseline, RSF.

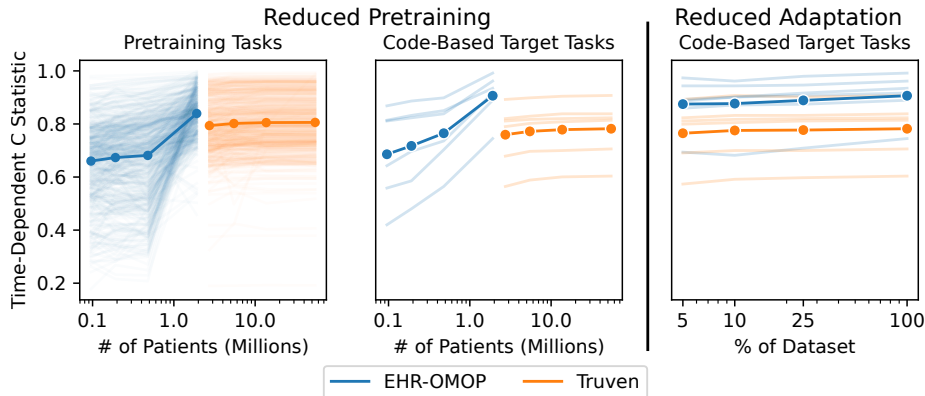


Figure 2: The time-dependent C statistic on both the pretraining tasks and code-based target tasks when MOTOR is either pretrained or adapted with less data. Average performance is plotted with a dark line while individual task performance is plotted faintly. Reduced Pretraining: Performance as a function of the amount of pretraining data. Reduced Adaptation: Performance as a function of the amount of data available for adaptation.

6 Discussion

We proposed a pretrained MOTOR model and showed that it can effectively solve a wide variety of risk prediction problems after being adapted to various time-to-event tasks. The process of pretraining allows us to use a high-parameter MOTOR model even in limited data settings. Our comprehensive experiments show that MOTOR-derived models outperform several state-of-the-art approaches and provide estimators with strong ranking and calibration performance across a range of clinical tasks. This success is owed to the novel TTE pretraining objective that enables MOTOR to learn sophisticated interactions and event distributions over 8,192 events.

Adapting MOTOR is scalable and computationally efficient, especially when combined with linear probing. After pretraining MOTOR once, the same model can be adapted for arbitrary downstream TTE tasks. Because linear probing only requires updating a small number of weights, it requires fewer labels and less compute. This allows us to train task-specific models up to ten times faster than RSF with only 5% of the labeled task data. The decreased computation and labeling costs resulting from MOTOR make TTE models more feasible in settings with limited resources.

This work has several limitations. First, pretraining MOTOR is computationally expensive, requiring several GPU days for EHR-OMOP and roughly two weeks for TRUVEN. Second, our experiments perform evaluations on subsampled target task datasets, which introduces censoring bias (as discussed in Appendix D), which might affect our results. Third, our handling of competing risks (censoring at death) may not be appropriate for every setting. Finally, our work does not address many of the societal impacts of using machine learning for healthcare, which are further discussed in Appendix J.

Medicine lags other machine learning disciplines in reproducibility measures [40, 63] due to challenges in releasing datasets and large pretrained models [67]. To help alleviate this (and allow others to build off our weights), we release MOTOR under a research DUA, which prohibits re-identifying patients as well as commercial and non-research use. We discuss further details, including

safeguards, in Appendix [K](#).

7 Conclusion

We have demonstrated that adapting a pretrained MOTOR model is an effective approach for a variety of TTE tasks, even in the presence of limited data. The use of pretraining, and in particular specialized TTE pretraining, allows us to learn a flexible deep neural network TTE model that can be adapted even in low sample settings and in limited compute resource situations where sophisticated modeling might not otherwise be viable.

Acknowledgements

This work was supported by R01 HL144555 from the National Heart, Lung, and Blood Institute (NHLBI).

References

- [1] A. M. Alaa and M. van der Schaar. Deep multi-task gaussian processes for survival analysis with competing risks. In *Proceedings of the 31st International Conference on Neural Information Processing Systems*, pages 2326–2334, 2017.
- [2] S. Athey, J. Tibshirani, and S. Wager. Generalized random forests. *Ann. Statist.*, pages 47(2): 1148–1178, 2019.
- [3] A. Avati, K. Jung, S. Harman, L. Downing, A. Ng, and N. H. Shah. Improving palliative care with deep learning. *BMC medical informatics and decision making*, 18(4):55–64, 2018.
- [4] A. Avati, T. Duan, S. Zhou, K. Jung, N. H. Shah, and A. Y. Ng. Countdown regression: Sharp and calibrated survival predictions. In *Uncertainty in Artificial Intelligence*, pages 145–155. PMLR, 2020.
- [5] R. Bommasani, D. A. Hudson, E. Adeli, R. Altman, S. Arora, S. von Arx, M. S. Bernstein, J. Bohg, A. Bosselut, E. Brunskill, et al. On the opportunities and risks of foundation models. *arXiv preprint arXiv:2108.07258*, 2021.
- [6] L. Breiman. Random forests. *Machine Learning*, pages 45: 5–32, 2001.
- [7] T. Chang, M. W. Sjoding, and J. Wiens. Disparate censorship & undertesting: A source of label bias in clinical machine learning, 2022. URL <https://arxiv.org/abs/2208.01127>.
- [8] Z. Che, S. Purushotham, K. Cho, D. Sontag, and Y. Liu. Recurrent neural networks for multivariate time series with missing values, 2016. URL <https://arxiv.org/abs/1606.01865>.
- [9] E. Choi, M. T. Bahadori, J. A. Kulas, A. Schuetz, W. F. Stewart, and J. Sun. Retain: An interpretable predictive model for healthcare using reverse time attention mechanism, 2016. URL <https://arxiv.org/abs/1608.05745>.
- [10] D. R. Cox. Regression models and life-tables. *Journal of the Royal Statistical Society: Series B (Methodological)*, 34(2):187–202, 1972.
- [11] R. D’Agostino and B.-H. Nam. Evaluation of the performance of survival analysis models: Discrimination and calibration measures. In *Advances in Survival Analysis*, volume 23 of *Handbook of Statistics*, pages 1–25. Elsevier, 2003. doi: [https://doi.org/10.1016/S0169-7161\(03\)23001-7](https://doi.org/10.1016/S0169-7161(03)23001-7). URL <https://www.sciencedirect.com/science/article/pii/S0169716103230017>.
- [12] A. M. Dai and Q. V. Le. Semi-supervised sequence learning. In C. Cortes, N. Lawrence, D. Lee, M. Sugiyama, and R. Garnett, editors, *Advances in Neural Information Processing Systems*, volume 28. Curran Associates, Inc., 2015. URL <https://proceedings.neurips.cc/paper/2015/file/7137debd45ae4d0ab9aa953017286b20-Paper.pdf>.

- [13] P. Dotson. Codes: What Are They, Why Are They Necessary, and How Are They Developed? *Adv Wound Care (New Rochelle)*, 2(10):583–587, Dec 2013.
- [14] T. Fernández, N. Rivera, and Y. W. Teh. Gaussian processes for survival analysis. *Advances in Neural Information Processing Systems*, 29, 2016.
- [15] M. Fornili, F. Ambrogi, P. Boracchi, and E. Biganzoli. Piecewise exponential artificial neural networks (peann) for modeling hazard function with right censored data. pages 125–136, 07 2014. ISBN 978-3-319-09041-2. doi: 10.1007/978-3-319-09042-9_9.
- [16] M. Friedman. Piecewise exponential models for survival data with covariates. *The Annals of Statistics*, 10(1):101–113, 1982.
- [17] Y. Gao and Y. Cui. Clinical time-to-event prediction enhanced by incorporating compatible related outcomes. *PLOS Digit Health*, 1(5), 2022.
- [18] M. A. Gianfrancesco, S. Tamang, J. Yazdany, and G. Schmajuk. Potential biases in machine learning algorithms using electronic health record data. *JAMA Intern Med*, 178(11):1544–1547, Nov 2018.
- [19] C. Guo, G. Pleiss, Y. Sun, and K. Q. Weinberger. On calibration of modern neural networks. *CoRR*, abs/1706.04599, 2017. URL <http://arxiv.org/abs/1706.04599>.
- [20] L. L. Guo, E. Steinberg, S. L. Fleming, J. Posada, J. Lemmon, S. R. Pfohl, N. Shah, J. Fries, and L. Sung. EHR foundation models improve robustness in the presence of temporal distribution shift. *Scientific Reports*, 13(1):3767, 2023.
- [21] F. E. Harrell, R. M. Califf, D. B. Pryor, K. L. Lee, and R. A. Rosati. Evaluating the yield of medical tests. *Jama*, 247(18):2543–2546, 1982.
- [22] N. Hartman, S. Kim, K. He, and J. D. Kalbfleisch. Pitfalls of the concordance index for survival outcomes. *Statistics in Medicine*, n/a(n/a). doi: <https://doi.org/10.1002/sim.9717>. URL <https://onlinelibrary.wiley.com/doi/abs/10.1002/sim.9717>.
- [23] P. J. Heagerty and Y. Zheng. Survival model predictive accuracy and roc curves. *Biometrics*, 61(1):92–105, 2005.
- [24] IBM Watson. IBM marketscan research databases for life sciences researchers, 2018. <https://www.ibm.com/downloads/cas/ONKLE57Y>.
- [25] J. Irvin, P. Rajpurkar, M. Ko, Y. Yu, S. Ciurea-Ilcus, C. Chute, H. Marklund, B. Haghgoo, R. L. Ball, K. S. Shpanskaya, J. Seekins, D. A. Mong, S. S. Halabi, J. K. Sandberg, R. Jones, D. B. Larson, C. P. Langlotz, B. N. Patel, M. P. Lungren, and A. Y. Ng. Chexpert: A large chest radiograph dataset with uncertainty labels and expert comparison. *CoRR*, abs/1901.07031, 2019. URL <http://arxiv.org/abs/1901.07031>.
- [26] H. Ishwaran, U. Kogalur, E. Blackstone, and et al. Random survival forests. *Ann Appl Stat*, pages 2(3):841–860, 2008.

- [27] H. Jing and A. J. Smola. Neural survival recommender. In *Proceedings of the Tenth ACM International Conference on Web Search and Data Mining, WSDM '17*, page 515–524, New York, NY, USA, 2017. Association for Computing Machinery. ISBN 9781450346757. doi: 10.1145/3018661.3018719. URL <https://doi.org/10.1145/3018661.3018719>.
- [28] J. L. Katzman, U. Shaham, A. Cloninger, J. Bates, T. Jiang, and Y. Kluger. DeepSurv: Personalized treatment recommender system using a cox proportional hazards deep neural network. *BMC Medical Research Methodology*, 18(1), feb 2018. doi: 10.1186/s12874-018-0482-1. URL <https://doi.org/10.1186/s12874-018-0482-1>.
- [29] M. Kohler, K. Máthé, and M. Pintér. Prediction from randomly right censored data. *Journal of Multivariate Analysis*, 80(1):73–100, 2002.
- [30] F. Konietzschke and M. Pauly. Bootstrapping and permuting paired t-test type statistics. *Statistics and Computing*, 24(3):283–296, Jan. 2013. doi: 10.1007/s11222-012-9370-4. URL <https://doi.org/10.1007/s11222-012-9370-4>.
- [31] P. Kopper, S. Pölsterl, C. Wachinger, B. Bischl, A. Bender, and D. Rügamer. Semi-structured deep piecewise exponential models. *CoRR*, abs/2011.05824, 2020. URL <https://arxiv.org/abs/2011.05824>.
- [32] A. Kumar, A. Raghunathan, R. M. Jones, T. Ma, and P. Liang. Fine-tuning can distort pretrained features and underperform out-of-distribution. In *International Conference on Learning Representations*, 2022. URL <https://openreview.net/forum?id=UYneFzXSJWh>.
- [33] H. Kvamme and O. Borgan. Continuous and discrete-time survival prediction with neural networks. *Lifetime Data Anal.*, 27(4):710–736, Oct 2021.
- [34] P. C. Lambert, P. W. Dickman, C. P. Nelson, and P. Royston. Estimating the crude probability of death due to cancer and other causes using relative survival models. *Statistics in medicine*, 29(7-8):885–895, 2010.
- [35] R. C. Li, S. M. Asch, and N. H. Shah. Developing a delivery science for artificial intelligence in healthcare. *NPJ Digit Med*, 3:107, 2020.
- [36] Y. Li, J. Wang, J. Ye, and C. K. Reddy. A multi-task learning formulation for survival analysis. In *Proceedings of the 22nd ACM SIGKDD International Conference on Knowledge Discovery and Data Mining, KDD '16*, page 1715–1724, New York, NY, USA, 2016. Association for Computing Machinery. ISBN 9781450342322. doi: 10.1145/2939672.2939857. URL <https://doi.org/10.1145/2939672.2939857>.
- [37] Y. Li, S. Rao, J. R. A. Solares, A. Hassaine, D. Canoy, Y. Zhu, K. Rahimi, and G. Salimi-Khorshidi. Behrt: Transformer for electronic health records, 2019. URL <https://arxiv.org/abs/1907.09538>.
- [38] Y.-K. Lin, H. Chen, R. A. Brown, S.-H. Li, and H.-J. Yang. Time-to-event predictive modeling for chronic conditions using electronic health records. *IEEE Intelligent Systems*, 29(3):14–20, 2014.
- [39] E. Martinsson. *Wtte-rnn: Weibull time to event recurrent neural network*. PhD thesis, Chalmers University of Technology & University of Gothenburg, 2016.

- [40] M. B. McDermott, S. Wang, N. Marinsek, R. Ranganath, L. Foschini, and M. Ghassemi. Reproducibility in machine learning for health research: Still a ways to go. *Science Translational Medicine*, 13(586):eabb1655, 2021.
- [41] R. Miotto, L. Li, B. A. Kidd, and J. T. Dudley. Deep patient: An unsupervised representation to predict the future of patients from the electronic health records. *Sci Rep*, 6:26094, May 2016.
- [42] S. J. Nelson, K. Zeng, J. Kilbourne, T. Powell, and R. Moore. Normalized names for clinical drugs: RxNorm at 6 years. *J Am Med Inform Assoc*, 18(4):441–448, 2011.
- [43] OHDSI. *The Book of OHDSI: Observational Health Data Sciences and Informatics*. OHDSI, 2019. ISBN 9781088855195. URL <https://books.google.com/books?id=JxpnzQEACAAJ>.
- [44] W. H. Organization. ICD-10 : International statistical classification of diseases and related health problems : Tenth revision, 2004.
- [45] J. M. Overhage, P. B. Ryan, C. G. Reich, A. G. Hartzema, and P. E. Stang. Validation of a common data model for active safety surveillance research. *Journal of the American Medical Informatics Association*, 19(1):54–60, 2012.
- [46] C. Pang, X. Jiang, K. S. Kalluri, M. Spotnitz, R. Chen, A. Perotte, and K. Natarajan. Cehr-bert: Incorporating temporal information from structured ehr data to improve prediction tasks. In S. Roy, S. Pfohl, E. Rocheteau, G. A. Tadesse, L. Oala, F. Falck, Y. Zhou, L. Shen, G. Zamzmi, P. Mugambi, A. Zirikly, M. B. A. McDermott, and E. Alsentzer, editors, *Proceedings of Machine Learning for Health*, volume 158 of *Proceedings of Machine Learning Research*, pages 239–260. PMLR, 04 Dec 2021. URL <https://proceedings.mlr.press/v158/pang21a.html>.
- [47] A. Perianez, A. Saas, A. Guitart, and C. Magne. Churn prediction in mobile social games: Towards a complete assessment using survival ensembles. In *2016 IEEE International Conference on Data Science and Advanced Analytics (DSAA)*. IEEE, oct 2016. doi: 10.1109/dsaa.2016.84. URL <https://doi.org/10.1109%2Fdsaa.2016.84>.
- [48] M. E. Peters, M. Neumann, M. Iyyer, M. Gardner, C. Clark, K. Lee, and L. Zettlemoyer. Deep contextualized word representations. In *Proceedings of the 2018 Conference of the North American Chapter of the Association for Computational Linguistics: Human Language Technologies, Volume 1 (Long Papers)*, pages 2227–2237, New Orleans, Louisiana, June 2018. Association for Computational Linguistics. doi: 10.18653/v1/N18-1202. URL <https://aclanthology.org/N18-1202>.
- [49] A. Radford, J. Wu, R. Child, D. Luan, D. Amodei, and I. Sutskever. Language models are unsupervised multitask learners. 2019.
- [50] C. Raffel, N. Shazeer, A. Roberts, K. Lee, S. Narang, M. Matena, Y. Zhou, W. Li, and P. J. Liu. Exploring the limits of transfer learning with a unified text-to-text transformer. *J. Mach. Learn. Res.*, 21(1), jun 2022. ISSN 1532-4435.
- [51] A. R. Rajkomar, E. Oren, K. Chen, A. Dai, N. Hajaj, M. Hardt, P. J. Liu, X. Liu, J. Marcus, M. Sun, P. P. Sundberg, H. Yee, K. Zhang, Y. Zhang, G. Flores, G. Duggan, J. Irvine, Q. Le, K. Litsch, A. Mossin, J. J. Tansuwan, D. Wang, J. Wexler, J. Wilson, D. Ludwig, S. Volchenboum, K. Chou, M. Pearson, S. Madabushi, N. Shah, A. Butte, M. Howell, C. Cui,

- G. Corrado, and J. Dean. Scalable and accurate deep learning for electronic health records. *npj Digital Medicine*, 2018. URL <https://www.nature.com/articles/s41746-018-0029-1>.
- [52] L. Rasmy, M. Nigo, B. S. Kannadath, Z. Xie, B. Mao, K. Patel, Y. Zhou, W. Zhang, A. Ross, H. Xu, and D. Zhi. Covrnn—a recurrent neural network model for predicting outcomes of covid-19 patients: model development and validation using ehr data. *medRxiv*, 2021. doi: 10.1101/2021.09.27.21264121. URL <https://www.medrxiv.org/content/early/2021/09/29/2021.09.27.21264121>.
- [53] L. Rasmy, Y. Xiang, Z. Xie, C. Tao, and D. Zhi. Med-BERT: Pretrained contextualized embeddings on large-scale structured electronic health records for disease prediction. *npj Digital Medicine*, 4(1), May 2021. doi: 10.1038/s41746-021-00455-y. URL <https://doi.org/10.1038/s41746-021-00455-y>.
- [54] K. Ren, J. Qin, L. Zheng, Z. Yang, W. Zhang, L. Qiu, and Y. Yu. Deep recurrent survival analysis, 2018. URL <https://arxiv.org/abs/1809.02403>.
- [55] A. Roy, M. Saffar, A. Vaswani, and D. Grangier. Efficient content-based sparse attention with routing transformers. *Transactions of the Association for Computational Linguistics*, 9:53–68, 2021. doi: 10.1162/tacl_a_00353. URL <https://aclanthology.org/2021.tacl-1.4>.
- [56] J. Y. Ryu, M. Y. Lee, J. H. Lee, B. H. Lee, and K. S. Oh. DeepHIT: A deep learning framework for prediction of hERG-induced cardiotoxicity. *Bioinformatics*, 36(10):3049–3055, May 2020.
- [57] M. Schemper. Cox analysis of survival data with non-proportional hazard functions. *Journal of the Royal Statistical Society. Series D (The Statistician)*, 41(4):455–465, 1992. ISSN 00390526, 14679884. URL <http://www.jstor.org/stable/2349009>.
- [58] O. H. D. Sciences and Informatics. Chapter 5 standardized vocabularies, Jan 2021. URL <https://ohdsi.github.io/TheBookOfOhdsi/StandardizedVocabularies.html>.
- [59] C. E. Shannon. A mathematical theory of communication. *The Bell System Technical Journal*, 27: 379–423, 1948. URL <http://plan9.bell-labs.com/cm/ms/what/shannonday/shannon1948.pdf>.
- [60] I. Solaiman. The gradient of generative ai release: Methods and considerations. *arXiv preprint arXiv:2302.04844*, 2023.
- [61] E. Steinberg, K. Jung, J. A. Fries, C. K. Corbin, S. R. Pfohl, and N. H. Shah. Language models are an effective representation learning technique for electronic health record data. *Journal of Biomedical Informatics*, 113:103637, 2021.
- [62] J. Su, Y. Lu, S. Pan, A. Murtadha, B. Wen, and Y. Liu. Roformer: Enhanced transformer with rotary position embedding, 2021. URL <https://arxiv.org/abs/2104.09864>.
- [63] K. TSIMA. The reproducibility issues that haunt health-care ai. *Nature*, 613, 2023.
- [64] M. J. Van der Laan and J. M. Robins. *Unified methods for censored longitudinal data and causality*, volume 5. Springer, 2003.
- [65] Z. Wang and J. Sun. Survtrace: Transformers for survival analysis with competing events. *CoRR*, abs/2110.00855, 2021. URL <https://arxiv.org/abs/2110.00855>.

- [66] Y. Wen, M. F. Rahman, Y. Zhuang, M. Pokojovy, H. Xu, P. McCaffrey, A. Vo, E. Walser, S. Moen, and T. B. Tseng. Time-to-event modeling for hospital length of stay prediction for COVID-19 patients. *Mach Learn Appl*, 9:100365, Sep 2022.
- [67] M. Wornow, Y. Xu, R. Thapa, B. Patel, E. Steinberg, S. Fleming, M. A. Pfeffer, J. Fries, and N. H. Shah. The shaky foundations of clinical foundation models: A survey of large language models and foundation models for emrs. *arXiv preprint arXiv:2303.12961*, 2023.
- [68] W. C.-H. Wu, M.-Y. Yeh, and M.-S. Chen. Predicting winning price in real time bidding with censored data. In *Proceedings of the 21th ACM SIGKDD International Conference on Knowledge Discovery and Data Mining*, KDD '15, page 1305–1314, New York, NY, USA, 2015. Association for Computing Machinery. ISBN 9781450336642. doi: 10.1145/2783258.2783276. URL <https://doi.org/10.1145/2783258.2783276>.
- [69] H. Xu, Z. Fu, A. Shah, Y. Chen, N. B. Peterson, Q. Chen, S. Mani, M. A. Levy, Q. Dai, and J. C. Denny. Extracting and integrating data from entire electronic health records for detecting colorectal cancer cases. *AMIA Annu Symp Proc*, 2011:1564–1572, 2011.
- [70] X. Zeng, S. L. Linwood, and C. Liu. Pretrained transformer framework on pediatric claims data for population specific tasks. *Scientific Reports*, 12(1):3651, Mar 2022. ISSN 2045-2322. doi: 10.1038/s41598-022-07545-1. URL <https://doi.org/10.1038/s41598-022-07545-1>.

Appendices

Appendix A Hyperparameter Search Grids

Table S1: Hyperparameter search grids of methods under comparison in our experiments. The software version for implementing each method is also shown.

Hyperparameters	Values
Cox PH	
lambda	automatic
min_patients_per_feature	100, 1000
software_version	glmnet 4.1-6
DeepSurv	
dropout	0, 0.1
first_layer_size	32, 128, 256, 512
second_layer_size	32
learning_rate	10^{-3} , 10^{-4} , 10^{-5}
min_patients_per_feature	100, 1000
software_version	pycox 0.2.3
Random Survival Forests	
node_size	5, 15, 50, 100
min_time_bins	8, 16, 32
min_patients_per_feature	100, 1000
software_version	randomForestSRC 3.1.0
MOTOR	
dropout	0, 0.1
learning_rate	10^{-3} , 10^{-4} , 10^{-5}
num_time_bins	8, 16
survival_dim	256, 512
inner_dim	768
layers	6, 12
max_sequence_length	16,384
vocabulary_size	65,536

Appendix B Data Processing Details

We first harmonize TRUVEN by converting it to the Observational Medical Outcomes Partnership (OMOP) schema [45] (EHR-OMOP comes in the OMOP schema). We then process our datasets by converting all of the tables within the OMOP schema to a uniform timeline format of timestamped events, where each event is annotated with both the time and the clinical code for that event. We additionally perform some post-processing to correct several timestamp-related issues in the source data. In particular, we move billing codes to the end of visits to better reflect when those billing codes are clinically available and move all events annotated at 12:00 AM to 11:59 PM to better account for how 12:00 AM timestamps frequently represent day-level timestamps and we do not want to have that data available to models before the end of the day. We also adjust for events before birth by moving them to the date of birth.

In order to obtain unbiased evaluation metrics for the performance of methods, we randomly split our data into training, validation, and test sets, containing 70%, 15% and 15% of the patients in the dataset. In order to ensure stable splitting, we use an approximate hash-based splitting algorithm so that splits are stable across dataset versions. The training set is used for all model training, the validation set is used for hyperparameter selection, and the test set is used for out-of-sample evaluation.

Table S2 contains the number of patients and events in each split for both datasets.

Table S2: Dataset split details

Split Name	EHR-OMOP		TRUVEN	
	# Patients	# Events	# Patients	# Events
Training Set	1,910,887	3,149,948,337	54,721,282	8,976,493,594
Validation Set	409,704	672,623,024	11,719,566	1,922,762,263
Test Set	409,820	673,687,781	11,726,429	1,923,815,575

We also compute some summary statistics for both of our datasets, which are shown in Table S3.

Appendix C Compute Environment

Experiments are performed in a local on-prem university compute environment using 24 Intel Xeon 2.70GHz CPU cores and 8 Nvidia V100 GPUs. All compute environments supported HIPAA-compliant data protocols. Each pretraining and/or finetuning job is only assigned one V100 at a time.

Appendix D Target Task Subsampling

Our task definition, of predicting the time until a coded event given a year of history, would generate a single label per patient in our dataset. This produces millions of labels for EHR-OMOP (tens of millions for TRUVEN) and is not feasible to analyze with most existing TTE modeling approaches. In order to work around this, in our experiments, we use a simple subsampling strategy where we drop a fraction d of the censored examples in our dataset before modeling and evaluation. This

Table S3: Demographic statistics for EHR-OMOP and TRUVEN. All patients have unknown race in TRUVEN as race is not provided. Standard deviations are provided in parenthesis when applicable.

Statistic Name	EHR-OMOP	TRUVEN
Total Patients	2,730,411	78,167,277
Total Events	4,496,259,142	12,823,071,432
Average Events Per Patient	1,646.7 (7,356.3)	164.0 (241.8)
Average Age	42.4 (24.3)	35.9 (19.0)
% Male	45.1	45.0
% American Indian or Alaska Native	0.3	N/A
% Asian	15.7	N/A
% African American	3.5	N/A
% Native Hawaiian or Other Pacific Islander	1.0	N/A
% White	42.9	N/A
% Unknown	36.7	100

causes a non-uniform scaling of the hazard rates. However, this does not affect our primary results as the resulting hazard rate scaling bias is shared across all methods and the primary goal of this study is to evaluate the relative performance of different modeling approaches. Since we evaluate and train all models using the same subsampling, the censoring bias affects them in a similar manner and our ranking of models’ performance should not be impacted. We considered correcting for this bias with a weighting strategy [29, 64], but extreme weights induce unstable training. We additionally do one other step of subsampling, where if the number of labels is still over 200,000 despite the prior strategy, we simply select a random sample of 200,000 when training models.

Even though subsampling controls in principle shouldn’t affect our ranking of methods, it is still useful to derive the exact hazard rate scaling induced by it. Let $H_i(t)$ be the hazard rate for a particular time t and let $\widetilde{H}_i(t)$ be the hazard rate for a particular time t induced by our subsampling strategy. Equation 2 provides the ratio of $\widetilde{H}_i(t)$ and $H_i(t)$. Proof D is the derivation of that equation.

$$\frac{\widetilde{H}_i(t)}{H_i(t)} = \frac{1}{1 - d\mathbb{P}(C_i < T_i | C_i > t, T_i > t)} \quad (2)$$

Proof. The hazard in our original dataset before sampling is

$$\begin{aligned}
H_i(t) &= \frac{\mathbb{P}(T_i = t)}{\mathbb{P}(T_i > t)} \\
&= \frac{\mathbb{P}(T_i = t) \mathbb{P}(C_i > t)}{\mathbb{P}(T_i > t) \mathbb{P}(C_i > t)} \\
&= \frac{\mathbb{P}(T_i = t, C_i > t)}{\mathbb{P}(T_i > t, C_i > t)} \quad \text{assume } C_i \perp\!\!\!\perp T_i \\
&= \frac{\mathbb{P}(T_i = t, C_i > t)}{\mathbb{P}(C_i < T_i, C_i > t, T_i > t) + \mathbb{P}(C_i \geq T_i, C_i > t, T_i > t)}
\end{aligned}$$

The hazard in our dataset after sampling is

$$\begin{aligned}
\widetilde{H}_i(t) &= \frac{\mathbb{P}(T_i = t, C_i > t)}{(1-d) \mathbb{P}(C_i < T_i, T_i > t, C_i > t) + \mathbb{P}(C_i \geq T_i, T_i > t, C_i > t)} \\
&= \frac{\mathbb{P}(T_i = t, C_i > t)}{((1-d) \mathbb{P}(C_i < T_i | T_i > t, C_i > t) + \mathbb{P}(C_i \geq T_i | T_i > t, C_i > t)) \mathbb{P}(T_i > t, C_i > t)} \\
&= \frac{\mathbb{P}(T_i = t, C_i > t)}{((1-d) \mathbb{P}(C_i < T_i | T_i > t, C_i > t) + (1 - \mathbb{P}(C_i < T_i | T_i > t, C_i > t))) \mathbb{P}(T_i > t, C_i > t)} \\
&= \frac{\mathbb{P}(T_i = t, C_i > t)}{(1-d \mathbb{P}(C_i < T_i | T_i > t, C_i > t)) \mathbb{P}(T_i > t, C_i > t)} \\
&= \frac{H_i(t)}{1-d \mathbb{P}(C_i < T_i | T_i > t, C_i > t)}
\end{aligned}$$

Thus,

$$\frac{\widetilde{H}_i(t)}{H_i(t)} = \frac{1}{1-d \mathbb{P}(C_i < T_i | C_i > t, T_i > t)}$$

□

Appendix E Target Task Counts

Table S4: Task details for six code based tasks on EHR-OMOP and TRUVEN.

Task Name	ICD 10 Codes	EHR-OMOP		TRUVEN	
		# Cases	# Controls	# Cases	# Controls
Celiac Disease	K90.0	3,453	13,812	91,119	364,476
Heart Attack	I21.*	2,815	11,260	116,085	464,340
Lupus	M32.*	3,274	13,812	90,002	360,008
Pancreatic Cancer	C25.*	2,163	8,652	16,175	64,700
NAFLD	K76.0	22,013	88,052	666,345	2,665,380
Stroke	I63.*	11,855	47,420	43,338	173,352

Appendix F Evaluation Metrics Details

The time-dependent C statistic summarizes the ability of a predictive model to rank patients by risk based on their instantaneous hazard functions. Specifically, we apply the incident and dynamic definitions for the time-dependent sensitivity and specificity, respectively, following the choices in Heagerty and Zheng [23]:

$$\begin{aligned} \text{sen}^{\text{I}}(c, t) &= \mathbb{P}(S_i > c | dN_i^*(t) = 1) \\ \text{spe}^{\text{D}}(c, t) &= \mathbb{P}(S_i \leq c | N_i^*(t) = 0), \end{aligned}$$

where S_i is the predicted risk score for subject i . $N_i^*(t) = \mathbb{1}\{T_i \leq t\}$ and $dN_i^*(t) = N_i^*(t) - N_i^*(t-)$ follow the standard definitions of a counting process. Then, the concordance can be expressed as a weighted average of the area under the time-dependent receiver operating curve (ROC)

$$C_{td} = \frac{\int_t \text{AUC}(t) w(t) dt}{\int_t w(t) dt} \quad (3)$$

where $w(t) = f(t) \cdot S(t)$. $f(t)$ is the event rate at a particular time t and $S(t)$ is the survival probability at that time. Both $f(t)$ and $S(t)$ are estimated using the Kaplan-Meier estimator. $\text{AUC}(t)$ is the time-specific area under ROC and can be computed by integration, and ROC can be calculated using sen^{I} and spe^{D} with the standard formulation.

Note that the formula in Equation (3) is slightly modified from Heagerty and Zheng [23] because our dataset contains many events that happened at the exact same time due to some events having only day-level time resolution. Heagerty and Zheng [23] assumes that all event times are distinct thus the sum of the weights (the term in the denominator) is $\frac{1}{2}$. As we have many tied event times, we cannot make the same assumption and have to explicitly compute the denominator as $\int_t w(t) dt$.

Harrell’s C-index [21] is an alternative type of C statistic that summarizes the ability of a predictive model to rank patients. There are two primary limitations of the Harrell’s C-index that the time-dependent C statistic does not have [22]. First, Harrell’s C-index does not account for censoring so it will be biased when used for evaluating TTE modeling performance. Second, Harrell’s

C-index requires the predictive model to output a single risk per patient, as opposed to risk over time. This causes problems when evaluating non-proportional hazards models such as RSF and MOTOR that have time-varying relative risks. We adjust for this by using the average hazard for models with time-varying risks. This will underestimate the performance of RSF and MOTOR, but will allow us to apply this metric.

We then use the standard formulation for computing Harrell’s C-index. First, we find all possible pairs P , where one patient is known to have the event before another, and split that set into P_{correct} (if the higher risk patient has the event first), P_{tied} (if both patients have the same risk), and $P_{\text{incorrect}}$ (if the lower risk patient has the event first).

$$C_H = \frac{P_{\text{correct}} + 0.5 \times P_{\text{tied}}}{P_{\text{correct}} + P_{\text{tied}} + P_{\text{incorrect}}} \quad (4)$$

The Nam-D’Agostino (ND) calibration metric [11] is constructed based on the idea that the survival probability estimates, $\hat{S}(t) = P(T_i > t)$, for a particular time t should be calibrated with respect to the number of observed survivors past that time point, which is not available in censored data, thus we estimate it using the Kaplan-Meier estimator per D’Agostino and Nam [11]. First, the data is sorted by $\hat{S}(t)$ given by a model and split into M equal size risk bins, where $\overline{p(t)}_m$ is the average value of $\hat{S}(t)$ within bin m . Second, a KM estimator is fit within each risk bin for computing actual survival probabilities. Finally, the squared difference between the expected and actual values is computed and summed across bins. The resulting statistic is χ^2 with $M - 1$ degrees of freedom. In principle, you can run hypotheses tests using this statistic, but we instead directly report and compare the raw statistic

$$\chi^2(t) = \sum_{m=1}^M \frac{[KM(t)_m - \overline{p(t)}_m]^2 n_m}{\overline{p(t)}_m(1 - \overline{p(t)}_m)}, \quad (5)$$

where n_m is the number of observations in bin m and $n_1 = n_2 = \dots = n_M$. For all evaluations, we set t to the median event time. In addition, we make one minor modification to this metric in that we remove the n_m term in the numerator as we are primarily concerned about relative performance. n_m a constant factor that only depends on the number of patients for each task, and removing it makes it easier to compare results across target tasks.

The time-dependent C statistic and ND test become increasingly unstable as the censoring rate increases since they rely on Kaplan Meier estimators that themselves become unstable at higher censoring rates. As such, it is generally recommended to only compute these statistics on a subset of the possible times to reduce the variance of estimates. As suggested by Heagerty and Zheng [23], we use the time-restricted variants of these evaluation metrics by setting a time limit of the 90% percentile of observed event times and only perform evaluations up to that time point.

In order to accurately quantify statistical significance, we use the paired test-set bootstrap approach [30] to estimate the 95% confidence interval for the difference in model performance between MOTOR and every other method. For every target task, we resample our test set with replacement to obtain 1000 bootstrap samples. We then compute all metrics for all of our models on each bootstrap sample, subtracting MOTOR’s performance each time to obtain an estimate of how each method differs from MOTOR. We finally compute confidence intervals by extracting the 2.5% and 97.5% percentiles of the bootstrapped samples. All of our confidence intervals for the differences in performance between methods are reported in Appendix G.

Appendix G Confidence Intervals

Table S5: 95% confidence intervals of difference in time-dependent C statistic between MOTOR-Finetune and the other methods. Higher numbers are considered better for this metric. * indicates statistically significant entries at $p = 0.05$.

Method	Celiac	Heart Attack	Lupus	NAFLD	Pancretic Cancer	Stroke
EHR-OMOP						
Cox PH	[-0.140, -0.088]*	[-0.146, -0.105]*	[-0.113, -0.073]*	[-0.147, -0.129]*	[-0.093, -0.050]*	[-0.105, -0.086]*
DeepSurv	[-0.120, -0.076]*	[-0.079, -0.048]*	[-0.091, -0.056]*	[-0.070, -0.057]*	[-0.075, -0.035]*	[-0.052, -0.037]*
RSF	[-0.096, -0.051]*	[-0.067, -0.036]*	[-0.094, -0.057]*	[-0.068, -0.055]*	[-0.060, -0.023]*	[-0.041, -0.027]*
MOTOR-Scratch	[-0.131, -0.083]*	[-0.114, -0.073]*	[-0.081, -0.041]*	[-0.047, -0.037]*	[-0.114, -0.064]*	[-0.050, -0.036]*
MOTOR-Probe	[-0.010, 0.009]	[-0.008, 0.001]	[-0.020, -0.005]*	[-0.008, -0.002]*	[-0.006, 0.004]	[-0.004, 0.003]
MOTOR-Finetune	[0.000, 0.000]	[0.000, 0.000]	[0.000, 0.000]	[0.000, 0.000]	[0.000, 0.000]	[0.000, 0.000]
TRUVEN						
Cox PH	[-0.273, -0.251]*	[-0.051, -0.043]*	[-0.095, -0.085]*	[-0.069, -0.056]*	[-0.219, -0.203]*	[-0.107, -0.096]*
DeepSurv	[-0.048, -0.037]*	[-0.019, -0.013]*	[-0.034, -0.028]*	[-0.039, -0.028]*	[-0.036, -0.029]*	[-0.046, -0.038]*
RSF	[-0.062, -0.052]*	[-0.022, -0.017]*	[-0.037, -0.031]*	[-0.028, -0.019]*	[-0.039, -0.032]*	[-0.053, -0.045]*
MOTOR-Scratch	[-0.029, -0.021]*	[-0.011, -0.006]*	[-0.015, -0.011]*	[-0.015, -0.008]*	[-0.015, -0.010]*	[-0.023, -0.017]*
MOTOR-Probe	[-0.010, -0.004]*	[-0.003, 0.000]	[-0.008, -0.004]*	[-0.008, -0.002]*	[-0.011, -0.007]*	[-0.008, -0.004]*
MOTOR-Finetune	[0.000, 0.000]	[0.000, 0.000]	[0.000, 0.000]	[0.000, 0.000]	[0.000, 0.000]	[0.000, 0.000]

Table S6: 95% confidence intervals for the difference in MOTOR’s time-dependent C statistic on the code-based tasks when the pretraining objective is changed. We evaluate both a “next code” baseline as well as our proposed time-to-event objective. * indicates statistically significant entries at $p = 0.05$.

Objective	Celiac	Heart Attack	Lupus	NAFLD	Pancretic Cancer	Stroke
Next Code	[-0.045, -0.010]*	[-0.036, -0.013]*	[-0.034, -0.009]*	[-0.008, 0.000]	[-0.021, 0.010]	[-0.023, -0.013]*
Time-to-Event	[0.000, 0.000]	[0.000, 0.000]	[0.000, 0.000]	[0.000, 0.000]	[0.000, 0.000]	[0.000, 0.000]

Table S7: 95% confidence intervals for the difference in ND calibration between MOTOR-Finetune and other methods. Lower numbers are better for this metric. * indicates statistically significant entries at $p = 0.05$.

Method	Celiac	Heart Attack	Lupus	NAFLD	Pancretic Cancer	Stroke
EHR-OMOP						
Cox PH	[-0.123, 0.202]	[-0.005, 0.309]	[0.082, 0.473]*	[0.029, 0.114]*	[-0.174, 0.190]	[-0.062, 0.026]
DeepSurv	[-0.220, 0.058]	[-0.111, 0.165]	[-0.138, 0.115]	[2.564, 3.231]*	[-0.190, 0.171]	[-0.058, 0.019]
RSF	[-0.021, 0.390]	[-0.029, 0.329]	[-0.179, 0.116]	[-0.004, 0.088]	[0.064, 0.481]*	[0.005, 0.121]*
MOTOR-Scratch	[2.540, 10.180]*	[2.110, 10.715]*	[10.933, 51.137]*	[-0.013, 0.070]	[2.839, 19.885]*	[-0.020, 0.134]
MOTOR-Probe	[-0.202, 0.043]	[-0.147, 0.063]	[-0.179, 0.037]	[-0.059, -0.004]*	[-0.134, 0.047]	[-0.061, 0.021]
MOTOR-Finetune	[0.000, 0.000]	[0.000, 0.000]	[0.000, 0.000]	[0.000, 0.000]	[0.000, 0.000]	[0.000, 0.000]
TRUVEN						
Cox PH	[-0.147, -0.077]*	[0.036, 0.076]*	[0.070, 0.138]*	[0.130, 0.244]*	[0.350, 0.523]*	[0.059, 0.096]*
DeepSurv	[-0.093, -0.035]*	[-0.016, 0.010]	[18.721, 21.664]*	[0.001, 0.062]*	[-0.110, -0.046]*	[2.870, 3.455]*
RSF	[-0.076, -0.017]*	[0.014, 0.060]*	[-0.004, 0.047]	[0.281, 0.436]*	[-0.037, 0.036]	[-0.004, 0.043]
MOTOR-Scratch	[-0.139, -0.061]*	[0.004, 0.057]*	[-0.021, 0.014]	[0.019, 0.091]*	[-0.026, 0.033]	[0.026, 0.061]*
MOTOR-Probe	[-0.131, -0.064]*	[-0.014, 0.007]	[-0.021, 0.019]	[-0.022, 0.025]	[-0.081, -0.010]*	[-0.016, 0.006]
MOTOR-Finetune	[0.000, 0.000]	[0.000, 0.000]	[0.000, 0.000]	[0.000, 0.000]	[0.000, 0.000]	[0.000, 0.000]

Table S8: 95% confidence intervals of difference in Harrell C-index between MOTOR-Finetune and the other methods. Higher numbers are considered better for this metric. * indicates statistically significant entries at $p = 0.05$.

Method	Celiac	Heart Attack	Lupus	NAFLD	Pancretic Cancer	Stroke
EHR-OMOP						
Cox PH	[-0.122, -0.069]*	[-0.162, -0.117]*	[-0.107, -0.068]*	[-0.148, -0.129]*	[-0.120, -0.074]*	[-0.111, -0.088]*
DeepSurv	[-0.100, -0.056]*	[-0.059, -0.035]*	[-0.077, -0.050]*	[-0.061, -0.047]*	[-0.074, -0.041]*	[-0.045, -0.029]*
RSF	[-0.072, -0.033]*	[-0.056, -0.032]*	[-0.079, -0.045]*	[-0.079, -0.065]*	[-0.063, -0.024]*	[-0.053, -0.036]*
MOTOR-Scratch	[-0.089, -0.049]*	[-0.078, -0.046]*	[-0.077, -0.042]*	[-0.045, -0.036]*	[-0.087, -0.044]*	[-0.047, -0.034]*
MOTOR-Probe	[-0.017, 0.001]	[-0.011, -0.002]*	[-0.029, -0.016]*	[-0.012, -0.006]*	[-0.004, 0.001]	[-0.006, 0.000]
MOTOR-Finetune	[0.000, 0.000]	[0.000, 0.000]	[0.000, 0.000]	[0.000, 0.000]	[0.000, 0.000]	[0.000, 0.000]
TRUVEN						
Cox PH	[-0.292, -0.279]*	[-0.064, -0.055]*	[-0.110, -0.098]*	[-0.090, -0.076]*	[-0.218, -0.205]*	[-0.125, -0.112]*
DeepSurv	[-0.053, -0.043]*	[-0.021, -0.016]*	[-0.036, -0.030]*	[-0.040, -0.031]*	[-0.038, -0.031]*	[-0.049, -0.040]*
RSF	[-0.071, -0.061]*	[-0.027, -0.022]*	[-0.044, -0.037]*	[-0.039, -0.030]*	[-0.046, -0.039]*	[-0.054, -0.045]*
MOTOR-Scratch	[-0.024, -0.017]*	[-0.011, -0.007]*	[-0.010, -0.006]*	[-0.013, -0.007]*	[-0.016, -0.011]*	[-0.017, -0.011]*
MOTOR-Probe	[-0.018, -0.012]*	[-0.008, -0.005]*	[-0.013, -0.009]*	[-0.008, -0.004]*	[-0.018, -0.014]*	[-0.013, -0.009]*
MOTOR-Finetune	[0.000, 0.000]	[0.000, 0.000]	[0.000, 0.000]	[0.000, 0.000]	[0.000, 0.000]	[0.000, 0.000]

Appendix H Additional Experiments

H.1 Calibration Performance

Table S9 provides ND calibration results for both baselines and MOTOR on our six code-based tasks. MOTOR yields the best calibration for most of the tasks; however, the improvements are not statistically significant given the overlapping confidence intervals in Table S7. Of note is that the MOTOR-Scratch baseline has substantially worse calibration, which is a common failure mode for neural network models [19].

Table S9: ND calibration for the various methods on the full datasets on the code-based tasks. Smaller values indicate smaller calibration errors. Bolding indicates the best performing model.

Method	Dataset	Celiac	HA	Lupus	NAFLD	Cancer	Stroke
Cox PH	EHR-OMOP	0.167	0.214	0.373	0.121	0.141	0.031
DeepSurv	-	0.041	0.089	0.102	2.911	0.081	0.023
RSF	-	0.299	0.225	0.095	0.091	0.345	0.112
MOTOR-Scratch	-	4.970	3.990	23.882	0.077	7.104	0.083
MOTOR-Probe	-	0.045	0.029	0.059	0.019	0.046	0.032
MOTOR-Finetune	-	0.092	0.031	0.109	0.043	0.059	0.046
Cox PH	TRUVEN	0.029	0.068	0.122	0.205	0.503	0.093
RSF	-	0.064	0.048	0.039	0.381	0.081	0.032
DeepSurv	-	0.048	0.007	20.001	0.051	0.005	3.158
MOTOR-Scratch	-	0.013	0.034	0.015	0.067	0.086	0.058
MOTOR-Probe	-	0.014	0.007	0.017	0.017	0.037	0.010
MOTOR-Finetune	-	0.108	0.009	0.014	0.016	0.075	0.015

H.2 Harrell’s C-index

Table S10 provides Harrell C-index results for both baselines and MOTOR on our six code-based tasks. MOTOR yield the best Harrell C-index on all of the tasks and the differences are statistically significant (see Table S8 for the confidence intervals).

H.3 Performance on Text-based Tasks

One limitation of our primary code-based task set is that all of the tasks are defined with code-based labels, which might not generalize to a more diverse set of applications. In order to better evaluate performance on more diverse tasks, we define some additional tasks derived from clinical notes on EHR-OMOP (TRUVEN does not contain textual notes so cannot be used to create tasks). Irvin et al. [25] created labeling functions to extract imaging observations from chest x-ray radiology notes, designed and tested to identify 13 different categories including fractures, lung lesions, and the presence of support devices. We construct time-to-event tasks for each possible observation by predicting the time until one of these observations from the end of a random visit. For example, we construct an “Edema” task that predicts the time until a radiology note has a positive present

Table S10: Harrell’s C-index for all methods on the code-based tasks. Bolding indicates the best performing model.

Method	Dataset	Celiac	HA	Lupus	NAFLD	Cancer	Stroke
Cox PH	EHR-OMOP	0.704	0.758	0.790	0.727	0.798	0.777
DeepSurv	-	0.722	0.851	0.814	0.811	0.838	0.839
RSF	-	0.747	0.853	0.816	0.793	0.852	0.831
MOTOR-Scratch	-	0.730	0.837	0.819	0.824	0.830	0.836
MOTOR-Probe	-	0.792	0.891	0.855	0.856	0.894	0.873
MOTOR-Finetune	-	0.799	0.898	0.878	0.865	0.895	0.876
Cox PH	TRUVEN	0.500	0.779	0.746	0.805	0.635	0.687
DeepSurv	-	0.738	0.820	0.817	0.852	0.811	0.761
RSF	-	0.720	0.814	0.809	0.853	0.804	0.755
MOTOR-Scratch	-	0.765	0.830	0.842	0.878	0.833	0.792
MOTOR-Probe	-	0.771	0.833	0.839	0.882	0.830	0.795
MOTOR-Finetune	-	0.786	0.839	0.850	0.888	0.846	0.805

mention of “Edema”. The list of tasks and number of cases / controls for each task are detailed in Table S11. Note that these tasks are generally much larger than the code-based tasks.

Table S11: Task setup details for text based tasks on EHR-OMOP.

Task Name	# Cases	# Controls
Atelectasis	28,465	113,860
Cardiomegaly	15,528	62,112
Consolidation	15,678	62,712
Edema	38,619	154,476
Enlarged Cardiomediatinum	10,778	43,112
Fracture	51,011	204,044
Lung Lesion	77,848	311,392
Lung Opacity	75,688	302,752
Pleural Effusion	46,255	185,020
Pleural Other	6,362	25,448
Pneumonia	17,165	68,660
Pneumothorax	9,123	3,6492
Support Devices	91,498	365,992

Due to the vastly increased size of these datasets, we only, we only compare MOTOR-Probe, RSFs and Cox PH. Table S12 provides the C statistics of each evaluated method on each task.

Results are very similar to the main code-based tasks as the relative ranking of methods stays the same. MOTOR is better than RSF, which in turn is better than Cox PH. This confirms that MOTOR continues to perform well, even on a diverse out of range task set that is based on radiology text labels.

Table S12: Time-dependent C statistic for various methods on the text based tasks. Larger values indicate better ranking performance.

Task	Cox PH	RSF	MOTOR-Probe
Atelectasis	0.773	0.858	0.880
Cardiomegaly	0.778	0.873	0.899
Consolidation	0.787	0.857	0.895
Edema	0.724	0.804	0.841
Enlarged Cardiomedastinum	0.733	0.823	0.863
Fracture	0.680	0.753	0.777
Lung Lesion	0.741	0.804	0.824
Lung Opacity	0.739	0.825	0.858
Pleural Effusion	0.730	0.808	0.836
Pleural Other	0.754	0.840	0.856
Pneumonia	0.781	0.813	0.853
Pneumothorax	0.781	0.883	0.893
Support Devices	0.699	0.811	0.840

H.4 Time to Train

The ability to fit TTE models quickly is essential for a variety of scenarios such as interactive model training and limited resource environments. One of the main advantages of MOTOR is that almost all of the weights can be frozen during finetuning, which means that one can learn target task models very quickly by only computing gradients for the linear heads.

In order to evaluate model training time, we perform timing experiments to compare the state of the art, RSF, to MOTOR in the fast linear probe setting. To simplify our experimental setup, we ignore the cost of hyperparameter tuning and focus solely on the time to fit a single final target task models with the optimally determined hyperparameters. In order to estimate the time to train as a function of sample size, we perform all experiments on random subsets of the NALFD task with the EHR-OMOP dataset, varying the training set size with each run. We provide 16 CPU cores, one V100 GPU, and 100 GB of RAM on isolated machines to both RSFs and MOTOR.

Figure S1 plots the clock time for both methods as a function of the number of labels (with the farthest right point representing the size of the NALFD task). RSF is competitive in instances with fewer labels, where the overhead of MOTOR is slightly higher, but becomes much slower with increased label counts where the increased efficiency of MOTOR allows us to train target task models much more quickly. In the most extreme case, when we use the full NALFD task, MOTOR is 10x faster. We note this is a somewhat conservative time comparison that ignores the cost and additional workflow complexity of materializing RSFs’ feature matrix.

H.5 Performance of Pretraining Task

When MOTOR is being pretrained, we are implicitly training 8,192 piecewise exponential TTE models across a variety of medical codes. Assessing pretraining performance is important because it allows us to evaluate MOTOR’s performance on a wider variety of tasks than the limited subset we explicitly evaluated on. Figure S2 provides the time-dependent C statistic as a function of the

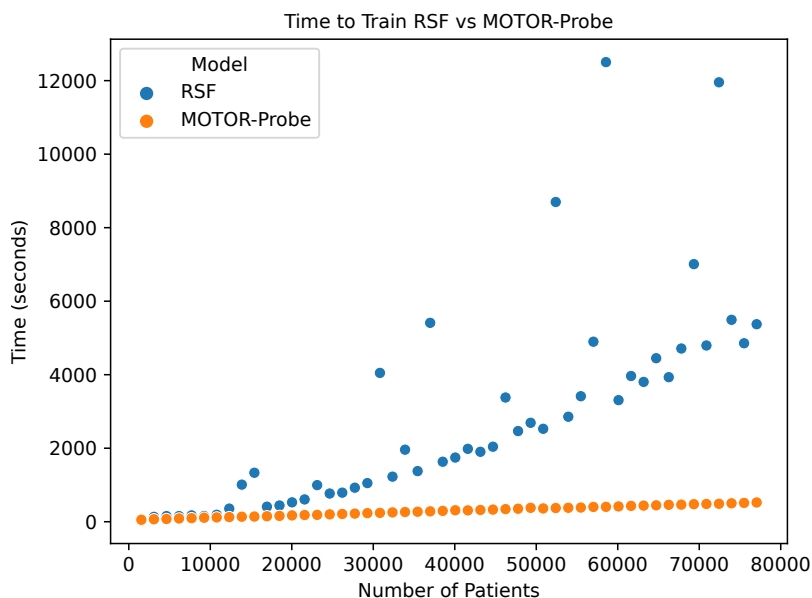


Figure S1: The time it takes to train target task models with MOTOR compared to RSF on varying amounts of patients.

amount of uncensored data for each task, with lines indicating the first quartile, median, and third quartile.

Performance on the pretraining tasks is strong across the vast majority of tasks, as indicated by the relatively high median C statistic of 0.842 for EHR-OMOP and 0.806 for TRUVEN. It is noteworthy that performance is also strong for highly censored tasks, even when only one in a thousand patients have an uncensored event.

H.6 Performance As a Function of Time Horizon

One interesting question is how the difference in ranking performance changes as a function of the time horizon. Figure S3 plots a heatmap of the difference between MOTOR and RSF across different time horizons. We see that the largest benefit of MOTOR is for short time horizons, but there is a general improvement across all time horizons. The decreased improvement in the later time horizons probably reflects a lower maximum potential performance for longer predictions as longer time horizons are fundamentally harder to predict.

H.7 Censoring Rate When Finetuning

In order to better evaluate less efficient TTE methods, we artificially lower the censoring rate to 80% for all of our tasks. However, many tasks in real life have a censoring rate higher than 80%. In order to evaluate in this setting, we perform some experiments where we remove some of the uncensored examples in our dataset to increase the censoring rate. For the sake of time and compute, we only perform this analysis on EHR-OMOP.

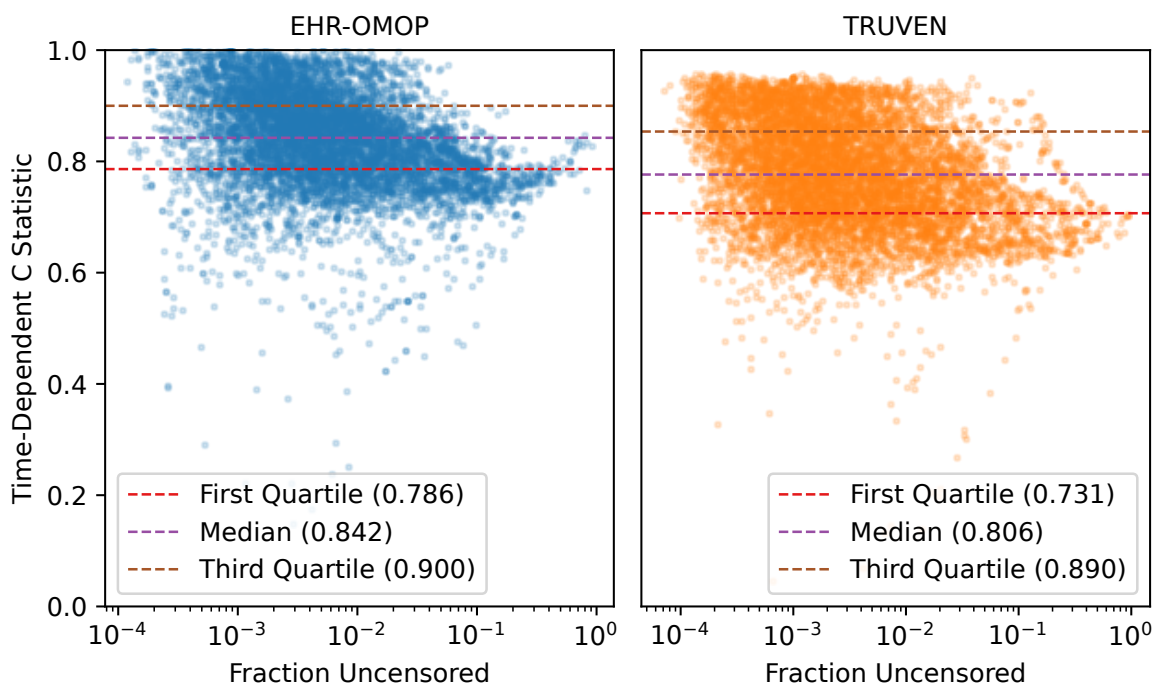


Figure S2: Pretraining task time-dependent C statistic as a function of the fraction of uncensored data. The dotted lines indicate specified quantiles for the C statistic.

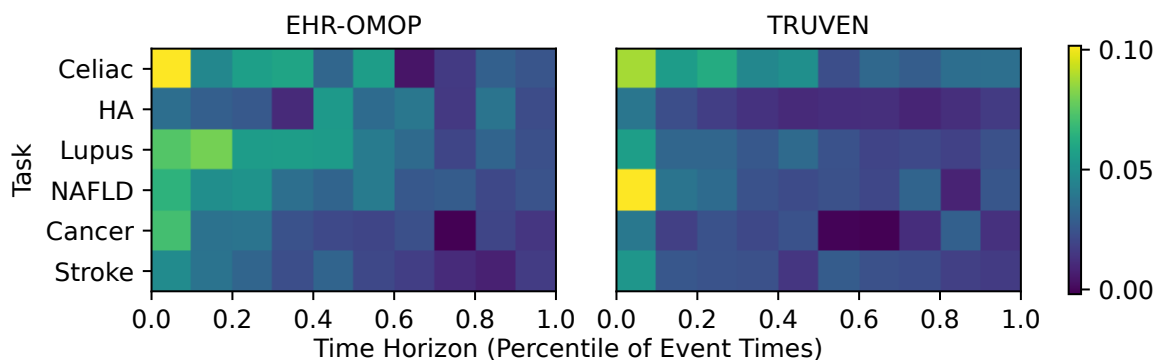


Figure S3: The difference in time-dependent C statistic between MOTOR-Finetune and RSF as a function of time-horizon.

Table S13 contains the time-dependent C statistics when MOTOR is fine-tuned using increasingly censored datasets. As the censoring rate increases, the performance decreases but only by an average of 1% even at 98% censored. This indicates that MOTOR performs fairly well even with highly censored data.

Table S13: Impact of the censoring rate when fine-tuning MOTOR on the time-dependent C statistic. We artificially increase the censoring rate by discarding increasing amounts of events. Experiments performed with EHR-OMOP.

% Censored	Celiac	Heart Attack	Lupus	NAFLD	Pancretic Cancer	Stroke
98%	0.792	0.882	0.844	0.851	0.863	0.863
95%	0.800	0.883	0.847	0.855	0.863	0.865
90%	0.801	0.884	0.850	0.858	0.864	0.870
80%	0.802	0.884	0.850	0.859	0.865	0.874

Appendix I Next Code Pretraining Task Setup

As a baseline, we construct a next code pretraining task in order to better understand the importance of our proposed time-to-event pretraining. Instead of predicting when a future target code occurs, we instead predict whether the code for the next event in the time series is equal to a particular target k . This is analogous to the standard autoregressive pretraining task in NLP language modeling. We formalize and implement this next code task as follows.

First, we construct a dictionary of potential target codes to predict. In order to ensure a fair comparison in our context of limited compute, we match the TTE pretraining setup by choosing the 8,192 highest entropy codes as our targets.

Given this fixed dictionary, we can construct a classification task. Each target k is assigned an embedding E_k that is the same width as the internal Transformer representation size. At each event j for every patient i , we compute a logit for each target k as the dot product of the final Transformer representation and the embedding $\text{logit}_{ijk} = R_{ij} \cdot E_k$. We can then train our model end-to-end with the standard cross-entropy classification likelihood loss. Let I_{ijk} be an indicator (1 if true, 0 if false) for whether the code for patient i at event j 's next event is equal to the target code k .

$$L(I|\text{logit}) = \prod_{i,j,k} I_{ijk} \cdot \sigma(\text{logit}_{ij})_k,$$

where $\sigma(\mathbf{z})_l = \frac{e^{z_l}}{\sum_{l'=1}^n e^{z_{l'}}$ is the standard softmax function.

This loss function can then be used to train a model end-to-end using the same setup as for MOTOR (with an Adam optimizer, decreasing learning weight schedule, etc.)

Appendix J Potential Societal Impacts

Machine learning in the context of healthcare comes with a variety of potential negative societal impacts that MOTOR models might worsen if used without a broader lens looking at the entire delivery set up [35]. One particular concern relevant to this work is that sophisticated risk models might be able to better learn the inequitable care patterns that are present in the input data due to various societal causes [18]. If a certain demographic is less likely or less able to interact with a hospital when they are sick, a model like MOTOR will systematically underestimate their risk, which could lead to reduced levels of care if MOTOR is used to guide treatment prioritization. Users of MOTOR (or any other ML guided risk-stratification regimen) have to employ bias minimization

during design and use evaluation strategies that can detect such problems to avoid perpetrating unjust practices.

Our work also comes with additional risks because we are releasing a large foundation model trained on patient records, which are de-identified but not intended to be publicly available in their native form. Discussion of those particular risks and our mitigation strategies are in Appendix K.

Appendix K MOTOR Model Release

We release a copy of the MOTOR weights trained on EHR-OMOP for external use to aid reproducibility and help others build off this work. The corresponding model card is in Appendix L. Due to the sensitivity of the data involved, we are doing a gated release [60] with a mandatory DUA to help prevent inappropriate use.

We also take a number of other steps to ensure the safety and privacy of the patients used during pretraining. First, we only train on de-identified, structured data to minimize any identifiable information that could leak into the model. All codes are restricted to a vocabulary defined by public medical ontologies and training data is de-identified to HIPAA standards to remove structured fields that are uniquely identifying, such as patients great than 90 years old. Second, all unique textual sequences in our model dictionaries (which are primarily categorical indicators like "Yes" or "No" for lab tests) have been manually verified to contain no PHI. Third, we release our model under a DUA that requires registering the identity of the user of the model and observing a policy where users will make no attempts to re-identify or extract patient level information from the model.

Appendix L Model Card for MOTOR

MOTOR is a pretrained time-to-event model for structured medical data.

L.1 Model description

MOTOR is a Transformer model pretrained using a time-to-event self-supervised objective on a large amount of de-identified EHR data. The pretraining objective is to predict the time-to-event of the highest entropy 8,192 medical codes in the source data. The resulting model learns representations that are useful for a variety of time-to-event modeling tasks

L.2 Intended use & limitations

The intended use of MOTOR is as a set of initial weights for fine-tuning a time-to-event model for a particular downstream use-case. MOTOR is intended for research-use only. MOTOR should in no way be used for the purposes of providing medical advice or to inform medical decision making in healthcare facilities or other organizations. This model is trained on EHR data, so it is probably most suited for creating EHR-based time-to-event models.

L.3 How to use

See `femr/tutorials/reference/2_apply_motor_model.py` within the code part of the supplement for a tutorial on how to use MOTOR.

L.4 Training data

MOTOR is trained on EHR-OMOP, a large de-identified hospital EHR database. EHR-OMOP contains 2.7 million patients (2.4 billion clinical events) spanning 2014 - 2022. EHR-OMOP follows the OMOP 5.4 database schema and standard.

L.5 Training procedure

MOTOR is trained for 10 epochs, with early stopping. Hyperparameters are noted within the log folder.

L.6 Evaluation results

MOTOR is evaluated by predicting the time until the first occurrence of a disease from a random visit in a patient’s timeline.

Time-dependent C statistics when MOTOR is finetuned on a variety of tasks:

Celiac Disease	Heart Attack	Lupus	NALFD	Pancreatic Cancer	Stroke
0.802	0.887	0.863	0.864	0.865	0.875